https://doi.org/10.2352/ISSN.2470-1173.2020.8.IMAWM-302
© 2020, Society for Imaging Science and Technology

Image Analytics for Food Safety

Min Zhao, School of Electrical and Computer Engineering, Purdue University, West Lafayette, IN, USA
Susana Diaz-Amaya, School of Materials Engineering, Purdue University, West Lafayette, IN, USA
Amanda J. Deering, Department of Food Science, Purdue University, West Lafayette, IN, USA
Lia Stanciu, School of Materials Engineering, Purdue University, West Lafayette, IN, USA
George T.-C. Chiu, School of Mechanical Engineering, Purdue University, West Lafayette, IN, USA
Jan P. Allebach, School of Electrical and Computer Engineering, Purdue University, West Lafayette, IN, USA

Abstract

Infectious diseases and environmental pollution caused by toxic chemical agents such as heavy metals are significant concerns in the global world. For example, Mercury (Hg) and Arsenic (As) have been recognized as chemical threats for human health. It is difficult to achieve multiple detections of different types of targets in lateral flow strips because of the multiple reagent requirements, while microfluidic paper-based analytical devices (μ-PADS) can provide independent channels and testing areas for colorimetric analysis. Herein, our group develops a low-cost, multiplexing, instrument-free, and simple paper-based fluidics biosensor to quantitatively determine Hg and As amounts in a linear range of 0 ppm - 30 ppm with a detection limit of 1 ppm and 2 ppm, respectively. We will present an overview of the results obtained with our fabrication process, the design of the preliminary pattern and image analysis of the responses in the test area, and the specificity test and stability test results.

Introduction

Nowadays, safety in food becomes critical. The main two types of threats related to food safety are foodborne pathogens and heavy metals [1][2]. One of the most common foodborne pathogens that can be found in our daily food is *E.coli* O157:H7. It can produce toxins that damage the lining of the intestine, cause bloody diarrhea, and sometimes result in kidney failure and even death. Human infections with *E.coli* O157:H7 are associated with the consumption of contaminated water and contaminated food, especially undercooked ground beef, milk and juice, raw fruits and vegetables. Moreover, such infections continue to occur regularly and result in severe disease and even loss of life. Therefore, it is crucial to develop an affordable, rapid, and simple method for detecting *E.coli* O157:H7.

To date, the widely used pathogen detections methods include culture-based counting, polymerase chain reaction (PCR), and enzyme-linked immunosorbent assay (ELISA). Among these methods, a plate culture takes 2-3 days to identify the suspected pathogens, and PCP involves laborious procedures. ELISA, which offers rapid detection, precision, high throughput, and low cost has attracted considerable interest; and it has a low detection limit of 10^4 CFU/mL [3]. To further push the limit of detection, our group incorporated printing and biomaterials technologies to develop inkjet printing lateral flow test strips for aptamer-based pathogen detection, and design an image analysis method to characterize and quantify the response in the biosensors to statistically prove that the detection limit of our biosensor is 10^2CFU/mL [4][5].

Beyond the foodborne pathogen *E.coli* O157:H7, we notice that the presence of heavy metals in food chains also poses a threat to public health. Heavy metals, including Mercury (Hg), Arsenic (As), Copper (Cu), and so on can be enriched in living tissue through food chains and proven harmful to human health at low concentrations. Currently, heavy metal detection methods used are Mass spectroscopy, Atomic Emission Spectroscopy, Potentiometric Methods, and so on [6][7][8][9]. These methods are sensitive but expensive and require expensive equipment, trained personnel and cannot support on-site detection. Therefore, rapid detection methods for heavy metal pollutants are more and more in demand.

During the last few decades, a wide variety of microfluidic paper-based biosensors have been successfully developed, demonstrating powerful tools for detecting food and environmental contamination [10] [11]. Microfluidic paper-based analytic devices (μPADs), developed in 2007 by Whiteside's team, have the characteristic of controlling a fluid motion via capillary force through specially designed microfluidic channel patterns on cellulose paper. As the major component of μPADs, cellulose papers with flexible porous fiber structure can wick liquids in small volumes without the need for external pumping equipment. The major task in the fabrication of μPADs is to create well-defined, millimeter-sized dimensional channels, comprising hydrophilic paper bounded by hydrophobic materials (wax or UV-curable inks) on cellulose papers. The heavy metals can be detected by gold nanoparticles (AuNPs) usually preloaded in reaction zones by providing colorimetric signals in biosensors. The colorimetric signals in the detection zones are commonly collected using a professional digital camera or a high-resolution scanner. Then, the color intensity of the signal in the captured images will be analyzed by some open source software. Unsurprisingly, μPADs have gained great attention due to their ease of use, low cost, amenability to colorimetric detection, and little test sample consumption.

To detect multiple targets in one test, which is hard to achieve with traditional lateral flow strips, our group focuses on developing a novel paper-based biosensor for colorimetric detection of two types of heavy metals: As and Hg. In this work, we first present paper-based devices fabricated by different technologies – different materials used to pattern hydrophobic walls across chromatography paper. Second, we propose preliminary patterns for multiple and multiplexed detection. Then, we detect the heavy metals at different concentrations to validate our approach. Finally, our optical system and image analysis pipeline guarantee to obtain consistent data acquisition captured by a mobile phone

camera, and deliver quantitative responses to correlate the colorimetric change of the biosensors to the concentration of the target substance.

Experimental Details

The major task in fabrication of μPADs is to create well-defined microfluidic channels, comprising hydrophilic paper bounded by hydrophobic materials. Among the available manufacturing technologies in the market, three techniques that are mainly employed are inkjet printing, wax screen printing, and UV-curable ink screen printing [12] [13][14].

To compare the different manufacturing methods, we pattern the paper with some materials (like wax, or UV-curable inks) to form the hydrophobic boundaries on hydrophilic paper in three different ways: (i) inkjet printing with UV-curable ink, (ii) wax screen printing, (iii) UV-curable ink screen printing.

The first way is to print nanoliter drops of UV-curable inks onto the substrate using a PipeJet Inkjet Printer (BioFluidiX, Freiburg, Germany). The hydrophobic wall is then generated by a UV lamp illuminating the printed UV-curable ink on the filter paper. Meanwhile, the unprinted regions retain their hydrophilic properties. We notice that the actual channel width is much smaller than the nominal width after the printing due to the long printing time; and the fact that the solvent of the UV-curable ink spreads faster than the pigment, as illustrated in Figure 1(a). Here, the pigment defines a channel of width 4.5 mm, whereas the channel defined by the spread of the solvent is only 1.5 mm wide. For wax screen printing, the wax is rubbed through the screen stencil with a squeegee to the filter paper. The printed paper is then heat-treated at 100 °C for 45 seconds; so that the wax can melt and spread vertically and laterally into the paper to form hydrophobic wax barriers. Finally, the printed paper is cooled to room temperature.

Figure 1(b) shows that the wax spreads unevenly after heating on a hot plate, therefore causing low-resolution printing. The result of the UV-curable ink screen printing shows that the diffusion of UV-curable ink is uniform, and the variation of the boundary width is smaller, as illustrated in Figure 1(c). Considering the requirements of cost and resolution, we choose UV-curable ink screen printing as the fabrication method for our fluidics paper-based biosensors.

Figure 1. *Results of three fabrication methods: (a) inkjet printing, (b) wax screen printing, (c) UV-curable ink screen printing.*

Materials

Paper-based devices are made from Whatman chromatography filter paper (Grade No.1, 20 cm width $\times$ 20 cm length). Screen stencils on aluminum frames with 230 polyester meshes (mesh opening 55 μm, Victory Factory, NY, USA), and UV curable inks (Ultra Switch UVSW180 and UVV6 Thinner, Maribu, Barcelona, Spain) are used to pattern the hydrophobic walls on the filter paper.

Fabrication of fluidic paper-based device

We design the digital pattern (mask) on a computer using graphics software (Adobe Illustrator CC 2019), and print it on transparent film with a laser printer (HP LaserJet 500 color MFP, USA) to make a stencil. Commercial screen-printing UV-curable inks are not suitable for patterning hydrophobic barriers on filter paper due to their high viscosity. To improve the penetrating ability of the UV-curable ink, one portion of UVSW 180 and three portions of UVV6 Thinner are mixed and stirred manually. The ink mixture is rubbed through the screen stencil with a squeegee to the filter paper. Owing to the porous structure of the filter paper, the low viscosity UV-curable inks can penetrate into the paper to form well-defined channels on the paper. Finally, the patterned papers are placed under a UV light (120 w/cm, 3 min) to be cured to form the hydrophobic walls.

Preliminary pattern design

To simplify our model, we start with a single target detection with two replicates. As shown in Figure 2, the fluidics paper-based device consists of two circular detection zones (diameter D), one central inlet for depositing sample solution, and two fluidics channels (whole length L, channel width d). Therefore, there are three parameters to be determined: d, L, and D.

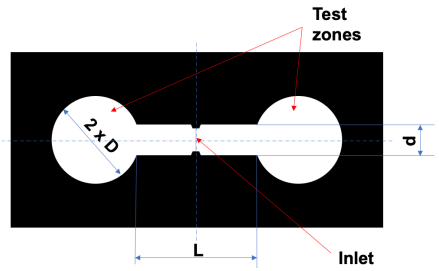

Figure 2. *Digital pattern with 2 test areas (the black area is the hydrophobic part generated by the UV-curable inks, the white area is paper).*

For channel width d, we have two main requirements: satisfy fast flow velocity and less solution loss in the path. We vary the values of d from 1 to 6 mm with an increment of 1 mm to observe the flow velocity and solution loss. Figure 3 shows the relationship between d and the flow distance of 100 μl DI water which flows fastest when the channel width d equals 4 mm.

Moreover, we choose the values of L, the channel length, by pipetting 20 μl aptamer-labels on two test zones to measure the smallest channel length that prevents overlap after the label diffusion. For the optimal value of D (circle diameter), we vary the diameter values from 8 mm to 12 mm with an increment of 2 mm, to choose the one that has the most visible color change by dropping the same amount of aptamer-labels on test areas.

To detect multiple pathogens in one test, we add two more test areas to the paper-based device. The details of the size and shape of our fluidics paper-based device are shown in Figure 4 (a). The diameter of all the circular pads is 8 mm, and the length of the entire fluidic channels is 20 mm, whereas the width is 4 mm.

Signal quantification

The common way to quantity the colorimetric detection of biosensors is to take pictures of the signal with an expensive, high

resolution and professional digital cameras or microscope, then analyze the images to obtain the color values using ImageJ software or Adobe software. Currently, mobile phones have become a popular and accessible platform for diagnostic systems due to the integration of cameras and light-sensors [15]. Motivated by these findings, we set up an optical system to capture images of different batches of biosensors by an optical system in a consistent and controlled illumination environment. Furthermore, the image analysis pipeline designed by our group is enabled to provide on-site recognition of the biosensors, characterization, and quantification of the colorimetric signals from the biosensors with minimal delay.

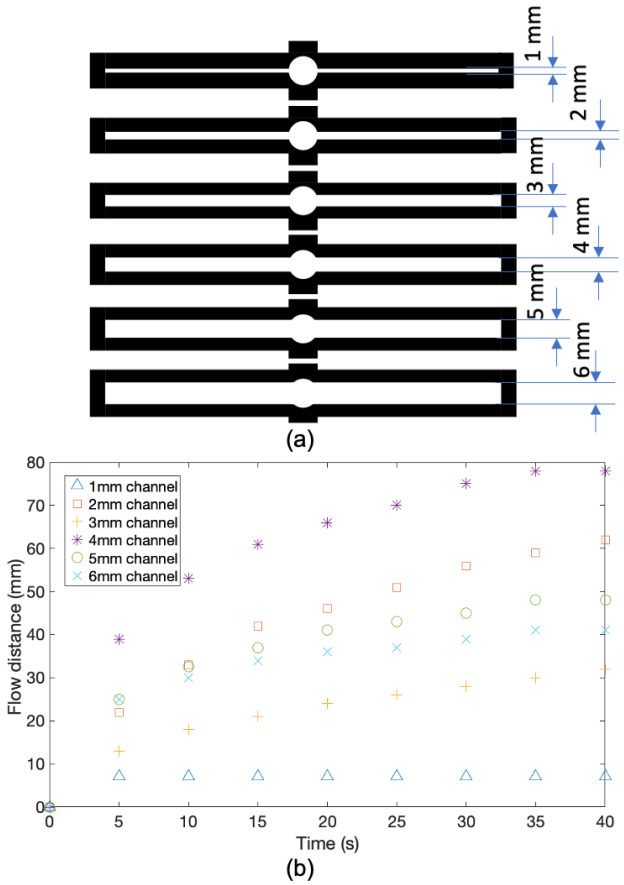

Figure 3. *The optimization of channel width d: (a) Digital patterns with different channel widths, (b) Flow distance of DI water on the channels with different widths. (Droplet volume = 100 µl).*

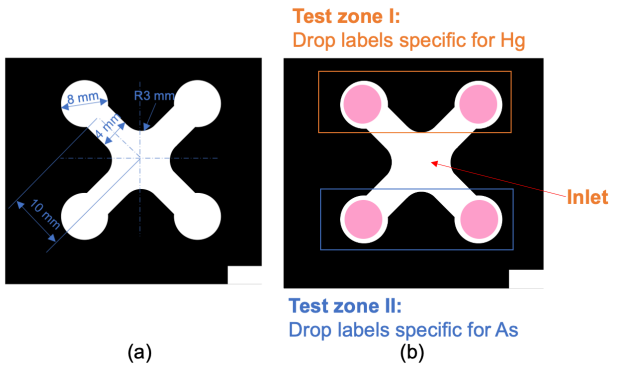

Figure 4. *The digital patterns: (a) Preliminary pattern design for fluidics paper-based devices with 4 test areas (detail of the size and shape), (b) The preloaded location of the two types of aptamer-functionalized particles (ssDNA-PEI-Au-Ps).*

Colorimetric detection

For the fabrication of the biosensor, 5 μl of the aptamer-functionalized particles (ssDNA-PEI-Au-Ps) binding to Hg^{2+} is added to each of the upper two circular pads, and 5 μl of apatamer-functionalized particles specific to As^{3+} is preloaded on each of the lower two circular pads. These four pads serve as the colorimetric labels. The biosensor is dried at room temperature for around 10 minutes. To detect the analytes in the test samples, 100 μl of test samples with nine different concentrations of As^{3+}, or Hg^{2+} were dropped in the inlet of the biosensors, from which the solution flowed evenly until reaching the testing areas. There is a colorimetric response in the presence of the target after the test solution interacts with the colorimetric label deposited on each of the testing areas. The color of the target testing areas gradually changes from light pink to deep purple as the concentration increases from 0 ppm to 30 ppm. Then, there is a drastic color change from deep gray to light gray for a higher concentration test, from 50 ppm to 100 ppm.

Data acquisition

The colorimetric signals in the detection zones are captured by our optical system, as illustrated in Figure 5(a). The optical system mainly consists of a photo studio booth (Amzdeal, purchased from Amazon.com) for providing the controlled D65 illumination environment, a mobile phone camera (iPhone 11 Pro Max, CA, USA), and a fixture to hold the mobile phone. One of the most significant reasons for poor quality images taken is shadows or uneven illumination. To verify the illumination stability of our optical system, ten images of a sheet of paper are taken under the same optical setting in the morning, and afternoon of the day, respectively. The photos are then converted to *CIE* $L^*a^*b^*$ color space, which is used to analyze the variance of the L^* values. As an example, Figure 5(b) shows the L^* value map for an image of the sheet of paper. From this example, it can be concluded that the illumination variance of the captured image is pretty low. Also, the standard deviation of the L^* values averaged over each page, and then averaged over the 10 pages is 0.19, which again, suggests that the illumination variation of the captured image is low.

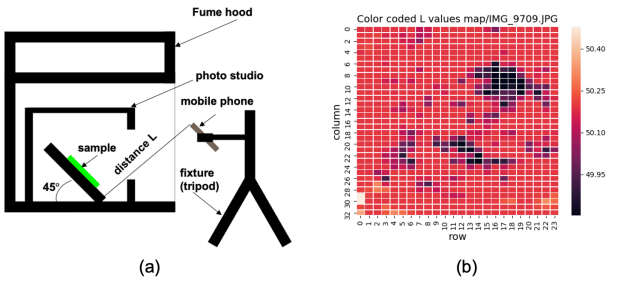

Figure 5. *(a) The schematic view of the optical system for capturing images, (b) The distribution of L^* values of the image of a sheet of paper.*

A. Template matching

For our experiment, we captured images of eight biosensors with each photograph. The approximate resolution of each biosensor is 400 × 400 pixels. Figure 6(a) shows one of the captured images obtained using our optical system.

The first step in our image analysis pipeline is to identify the region of the captured image corresponding to each of the 8 biosensors. To accomplish this task, we perform template matching [16]. One template image (400 × 400 pixels), including a fabricated biosensor, is chosen to recognize the positions of all biosensors in the source image by labeling all the detected positions of each biosensor using red squares (Figure 6(a)) and recording the centroid coordinates of each red square as shown in Figure 6(b). Unfortunately, after application of the template matching method to the captured images, the position of each biosensor is detected multiple times, as shown by the thick borders of red squares in Figure 6(a) and by each red pixel cluster in Figure 6(b), corresponding to one of the eight biosensors. We will refine our estimates of the biosensor locations using the K-means algorithm, as discussed next.

B. K-means clustering method

We generate a distribution of the centroids of the red squares, where the two dimensions are the pixel indices in the x and y direction, as shown in Figure 6(b). Each red cluster composed of some red dots in Figure 6(b) corresponds to all centroid positions of a biosensor detected by the template matching method. To refine our estimates of the biosensor locations, we then apply the K-means algorithm [17] to compute a centroid for each cluster, as shown by the blue dots in Figure 6(b). Finally, the individual biosensor images are cropped based on the blue squares determined by the blue dots and saved in TIFF format without compression, as illustrated in Figure 6(c).

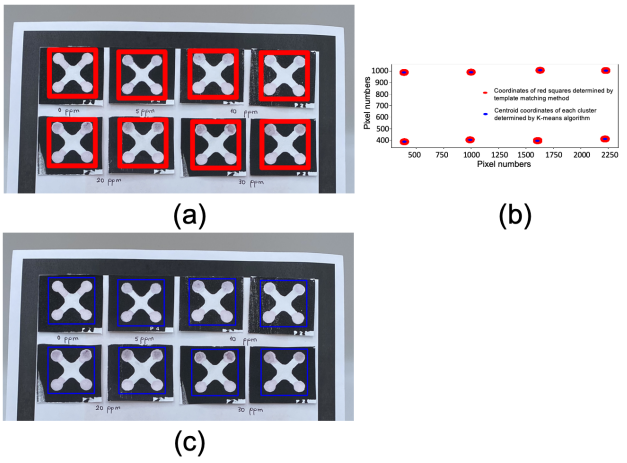

Figure 6. *The process of extracting the region of interest: (a) The template matching result (the thick borders of red squares show that each ROI has been recognized many times), (b) The distribution of the centroid coordinates (red dots) of the red squares, and the centroid coordinate (blue dot) for each red cluster, (c) The classification results after using K-means algorithm to partition the coordinates of the red squares into 8 partitions .*

Image analysis pipeline

After a region of interest is identified, the region of interest is further processed to obtain a quantified measurement of the results. We use image analysis methods to characterize the response of our fluidics paper-based devices to the heavy metals, due to colorimetric changes in the region of interest. We propose an image analysis method to assess the responses by using a mobile phone camera. In this approach, the metric that we use to characterize the responses in each circular detection zone is based on the average grayscale value, which is the average *CIE* ΔE value in the detection zone. Here, the ΔE value is calculated as the difference between the average L^* value of test area and the average L^* value of a region located in the central inlet. Our image analysis process involves two steps: segmentation of the detection zone or test area and colorimetric signal quantification.

Image segmentation

Image segmentation is one of the essential operations in image processing, in which an image is subdivided into several regions with the aid of pixel information, such as color, lightness, and texture. A number of automatic segmentation methods and unsupervised methods have been developed [18][19]. It is observed that the segmentation result can directly affect the subsequent analysis, and there is no universal or best image segmentation method because different images have different characteristics.

In this article, we focus on a hybrid segmentation approach based on Otsu's method and the K-means clustering method. The first step is to detect the whole channels of each biosensor using Otsu's method. Then, we apply the K-means clustering method to the channels obtained by the boundary detection to segment the test area from the white background. Finally, a morphological operation is applied to remove the noise and boundaries of the channels. The flow chart of the proposed segmentation method is illustrated in Figure 7.

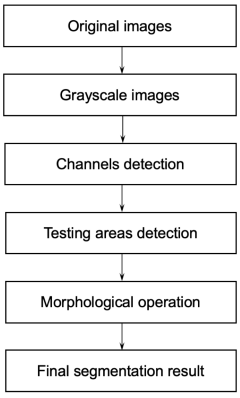

Figure 7. *Flow chart of the proposed segmentation method.*

A. Otsu's method

Otsu's thresholding method is one of the best-known methods for automatic image segmentation. Based on the histogram of a grayscale image, Otsu's method finds the optimal threshold t^* that maximizes the between-class variance.

To obtain the grayscale images, we transform the gamma-corrected sRGB values of each digital image (Figure 8(a)) to *CIE* $L^*a^*b^*$ color space, which has a visually uniform distribution of colors and is closer to human perception of color differences than is sRGB. After transformation, an image difference matrix ΔE of each test image is obtained by subtracting the test zone images from the average $L^*a^*b^*$ value in the central inlet of the biosensor using Equation (1),

$$\Delta E(i,j) = \sqrt{(L^*(i,j)-L^*_{avg})^2+(a^*(i,j)-a^*_{avg})^2+(b^*(i,j)-b^*_{avg})^2} \quad (1)$$

where (i,j) denotes the pixel indices and $\left(L^*_{avg}, a^*_{avg}, b^*_{avg}\right)$ is the average value in the central inlet. Then, we normalize the ΔE values of the images to the range [0, 255] to obtain our grayscale iamge for each biosensor, as shown in Figure 8(b).

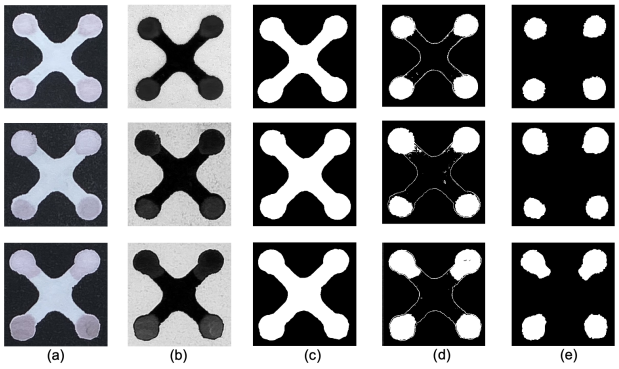

Figure 8. *Results of the proposed hybrid segmentation approach based on Otsu's method and the K-means clustering method: (a) Original sRGB images, (b) Grayscale images, (c) Channel detection results, (d) Testing areas detection results, (e) Final segmentation results after applying a morphological closing operation.*

Otsu's thresholding method works well in segmenting the channels from the black hydrophobic area because the histogram of each image, including the channels, has a strongly bimodal distribution. Figures 8(c) shows the channel segmentation results.

B. Feature selection and K-means clustering method

The following step is used to recognize the testing areas inside the channels. The color difference between the pads and the central inlet region increases as the detected concentration of the analyte increases.

The following features are selected as the input to K-means clustering method: $[L^*(i,j), a^*(i,j), b^*(i,j), \Delta E(i,j), w\cdot i, w\cdot j]$, where $L^*(i,j)$, $a^*(i,j)$, $b^*(i,j)$ are the pixel values in the *CIE* L^*, a^*, b^* channels. $\Delta E(i,j)$ is the grayscale values of each pixel. i, j are the pixel coordinates, and w is a weighting factor applied to these coordinates. In this case, w is chosen empirically to be 0.05. The number of clusters K equals 5 because there are four testing areas and a white background (filter paper).

After applying the K-means clustering method, we distinguish the four testing pads from the white background, as illustrated in Figure 8(d).

C. Morphological operation

The biosensors in Figure 8(d) show the presence of the boundaries of the channels and some noise. Morphological operations are widely applied to remove unnecessary features from images. The basic morphological operations widely used in image processing are erosion and dilation, which are performed over a neighborhood specified by a structuring element or a kernel [20]. To remove the boundaries of the channels and unwanted noise, a window size of 5×5 is chosen to do erosion followed by dilation, which is also called an opening operation. The result in Figure 8(e) shows that the opening operation effectively removes the undesired features in Figure 8(d).

The final segmentation results prove that our proposed hybrid segmentation combining Otsu's method and the K-means clustering method enables us to locate the testing areas accurately.

Qantification results

With the aid of the binary images, the position of the colorimetric responses in the testing areas can be defined. We use grayscale values as a metric, calculating average ΔE from the white reference ($[L^*, a^*, b^*] = [93.1927, -2.3147, -0.7811]$) of the response areas, to characterize the response of the paper-based devices.

Various concentrations of Hg^{2+} and As^{3+} are tested on the proposed fluidics paper-based biosensors. The detection of each concentration is repeated in at least six replicates, and the data is averaged. The analytical response ΔE is calculated after image processing and analysis. Figure 9(a) shows the colorimetric signal evolution versus various concentrations of As^{3+} from 0 ppm to 100 ppm. As illustrated in Figure 9(b), correlations can be seen between the ΔE values and the increasing concentrations of the analytes. According to the data collected, the variable ΔE and the As^{3+} concentration is found to be strongly correlated from 0 to 30 ppm. Furthermore, the results in Figure 9(b) show evidence that the limit of detection of our proposed biosensor is 2 ppm. Figure 9(c) shows the color evolution of the response for Hg^{2+} under increasing concentrations. The analytical response in Figure 9(d) shows the evidence of a linear correlation from 0 ppm to 50 ppm with a limit of detection of 1 ppm.

At the higher concentration of 100 ppm, there is a drastic color change from deep gray to light gray due to an aggregation effect of the aptamer-based particles (ssDNA-PEI-Au-Ps). The mechanism for forming these particles is induced-aggregation. So a higher concentration of the analytes can increase the particle aggregation effect, and grow the particle size. Then, they might start absorbing light at longer wavelengths (IR spectrum). Therefore, the visible wavelengths reflected from the aggregated particles will show a lighter color.

Our proposed biosensor has been shown to be able to effectively detect heavy metals Hg^{2+} and As^{3+} at a low concentration. To predict the biosensing performance of the proposed paper-based biosensor in complex water or food mixtures with various kinds of heavy metals, a specificity test focused on the most common heavy metals Cadmium (Cd), Iron (Fe), Magnesium (Mg), and Lead (Pb) with the concentrations of 50 ppm, is performed. The detection of each heavy metal with the same concentration is independently repeated in 6 replicates; and the data is averaged. The signal of the blank solution is used as a negative reference for comparing the colorimetric signal. The results in

Figure 10(a) show there is a visually large color difference in the testing areas between the targets and the non-targeted heavy metals. Also, Figure 10(b) demonstrates that Hg^{2+} and As^{3+} have the highest positive signal in the test groups after image processing and analysis. Therefore, the test results confirm that our proposed biosensor is highly specific to Hg^{2+} and As^{3+}.

To further evaluate the reliability and long-term stability of the response of the proposed biosensor to the analyte, we perform two sets of experiments to observe the colorimetric signal of the paper-based devices stored at room temperature for several weeks.

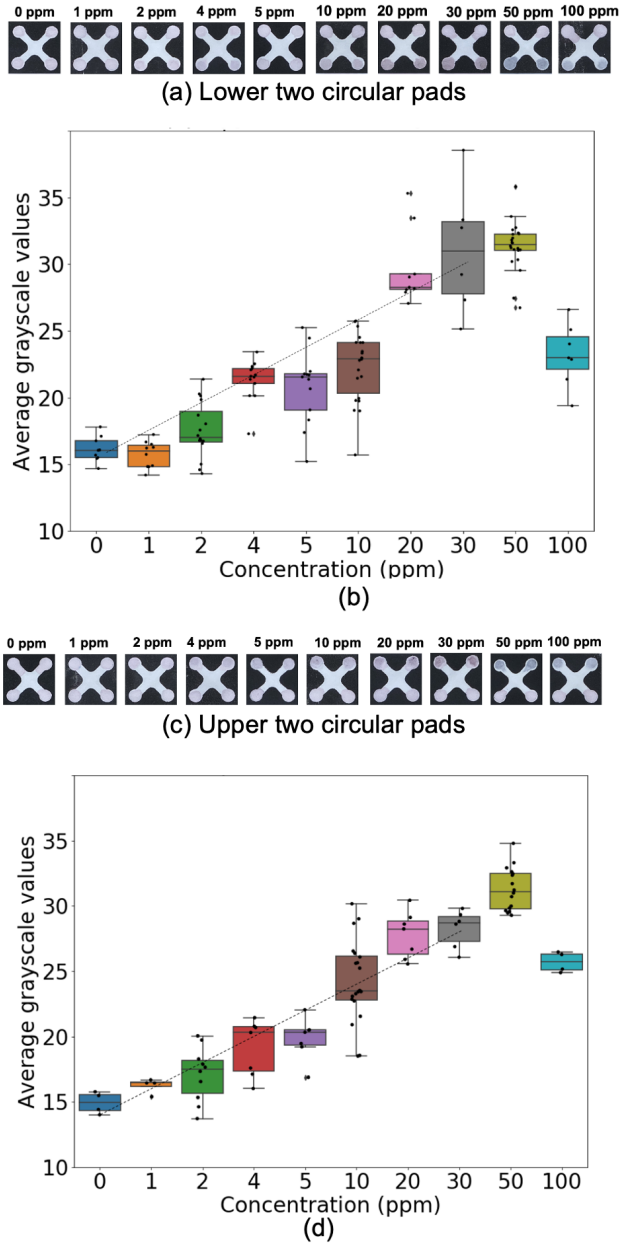

Figure 9. *(a) The colorimetric signal response to As^{3+}, (b) The correlation between ΔE values and the increasing concentrations of As^{3+}, (c) The colorimetric signal response to Hg^{2+}, (d) The correlation between ΔE values and the increasing concentrations of Hg^{2+}.*

The paper-based devices are prepared in different weeks, and one batch is used to evaluate the stability of the reagent by testing with the blank solution, the rest of the biosensors are used to test with Hg^{2+} at the concentration of 10 ppm. The difference between the signal for samples with blank solution and Hg^{2+} at 10 ppm is visually apparent and analytically significant at the end of the study period, as illustrated in Figures 11(a) and 11(b). These results demonstrate that the proposed paper-based biosensor is able to provide robust detection results for the analytes.

Conclusion

In this paper, we have developed a novel biosensor using a paper-based, microfluidic architecture. We explored three different printing technologies for fabricating these devices, and chose screen printing with UV cured inks for further development. We then conducted empirical studies to optimize the device geometry. Finally, we developed a complete image processing pipeline to enable detection of the presence of contaminants in the designed test areas.

Then, we showed that our biosensor can detect the presence of heavy metals (Mercury and Arsenic), and confirmed an Aptamer-based assay detection limit of 1 ppm, and 2 ppm, respectively, for these two contaminants. The relationship between the optical properties and the different concentrations of the target was also investigated. The specificity test and stability results prove that our proposed biosensor is highly specific and robust to the analytes.

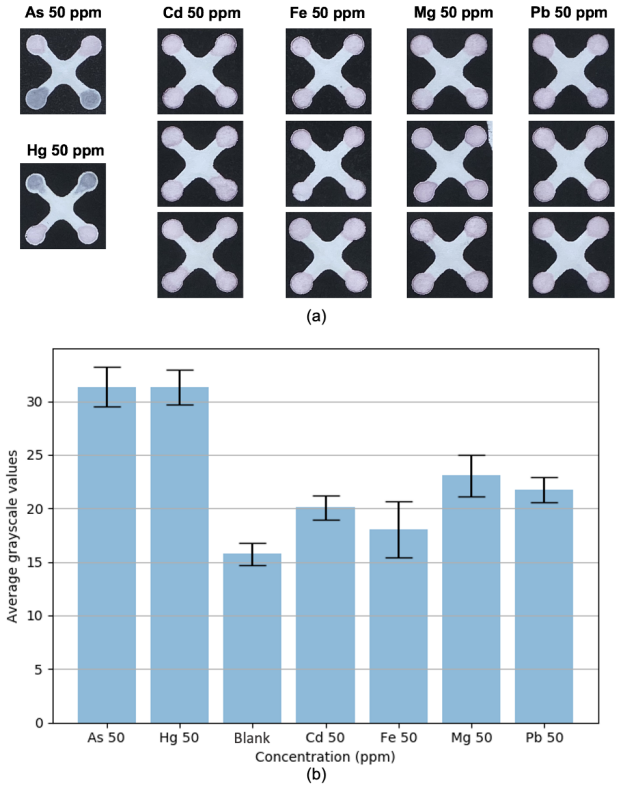

Figure 10. *The specificity test results of the proposed paper-based devices: (a) Images of the test results, (b) Box plot of the colorimetric signal of the test samples.*

Acknowledgments

This manuscript is based upon work supported by the U.S. Department of Agriculture, Agricultural Research Service, under Agreement No. 59-8072-6-001. Any opinions, findings, conclusion, or recommendations expressed in this publication are those of the author(s) and do not necessarily reflect the view of the U.S. Department of Agriculture.

References

[1] H.L. DuPont, The growing threat of foodborne bacterial enteropathogens of animal origin, Clinical Infectious Diseases, pg. 1353. (2007).

[2] G. Mance, Pollution threat of heavy metals in aquatic environments, Springer Science & Business Media. (2012).

[3] M. Feng, Q. Yong, W. Wang, H. Kuang, L. Wang, and C. Xu, Development of a monoclonal antibody-based ELISA to detect Escherichia coli O157: H7, Food and Agricultural Immunology, pg. 481. (2013).

[4] S. Díaz-Amaya, M. Zhao, L.K. Lin, C. Ostos, J.P. Allebach, G.T.C. Chiu, A.J. Deering, and L.A. Stanciu, Inkjet printed nanopatterned aptamer-based sensors for improved optical detection of foodborne pathogens, Small, p. 1805342. (2019).

[5] M. Zhao, S. Diaz Amaya, S.A. Jin, L.K. Lin, A.J Deering, L. Stanciu, G.T.C Chiu, and J.P. Allebach, Inkjet Printing platforms for DNA-based pathogen detection, NIP & Digital Fabrication Conference, pg. 107. (2018).

[6] R. Flamini, and A. Panighel, Mass spectrometry in grape and wine chemistry. Part II: The consumer protection, Mass Spectrometry Reviews, pg. 741. (2006).

[7] P. Pohl, Determination of metal content in honey by atomic absorption and emission spectrometries, TrAC Trends in Analytical Chemistry, pg. 117. (2009).

[8] J. Wang, G. Liu, and A. Merkoçi, Electrochemical coding technology for simultaneous detection of multiple DNA targets, Journal of the American Chemical Society, pg. 3214. (2003).

[9] M.R. Saidur, A.A. Aziz, and W.J. Basirun, Recent advances in DNA-based electrochemical biosensors for heavy metal ion detection: a review, Biosensors and Bioelectronics, pg. 125. (2017).

[10] L.S.A Busa, S. Mohammadi, M. Maeki, A. Ishida, H. Tani, and M. Tokeshi, Advances in microfluidic paper-based analytical devices for food and water analysis, Micromachines, pg. 86. (2016).

[11] Y. Zhang, P. Zuo, and B.C. Ye, A low-cost and simple paper-based microfluidic device for simultaneous multiplex determination of different types of chemical contaminants in food, Biosensors and Bioelectronics, pg. 14. (2015).

[12] C. Xu, L. Cai, M. Zhong, and S. Zheng, Low-cost and rapid prototyping of microfluidic paper-based analytical devices by inkjet printing of permanent marker ink, Rsc Advances, pg. 4770. (2015).

[13] W. Dungchai, O. Chailapakul, and C.S. Henry, A low-cost, simple, and rapid fabrication method for paper-based microfluidics using wax screen-printing, Analyst, pg. 77. (2011).

[14] P.J. Lamas-Ardisana, P. Casuso, I. Fernandez-Gauna, G. Martínez-Paredes, E. Jubete, L. Añorga, G. Cabañero, and H.J. Grande, Disposable electrochemical paper-based devices fully fabricated by screen-printing technique, Electrochemistry Communications, pg. 25. (2017).

[15] A.K. Yetisen, J.L. Martinez-Hurtado, A. Garcia-Melendrez, F. da Cruz Vasconcellos, and C.R. Lowe, A smartphone algorithm with inter-phone repeatability for the analysis of colorimetric tests, Sensors and Actuators B: Chemical, pg. 156. (2014).

[16] R. Brunelli, Template matching techniques in computer vision: theory and practice, John Wiley & Sons. (2009).

[17] Hartigan, J.A. and Wong, M.A., Algorithm AS 136: A k-means clustering algorithm, Journal of the Royal Statistical Society. Series C (Applied Statistics), pg. 100. (1979).

[18] N. Otsu, A threshold selection method from gray-level histograms, IEEE Transactions on Systems, Man, and Cybernetics, pg. 62. (1979).

[19] W. Khan, Image segmentation techniques: A survey, Journal of Image and Graphics, pg. 166. (2013).

[20] Q. Chen, P. Gong, D. Baldocchi, and G. Xie, Filtering airborne laser scanning data with morphological methods, Photogrammetric Engineering & Remote Sensing, pg. 175. (2007).

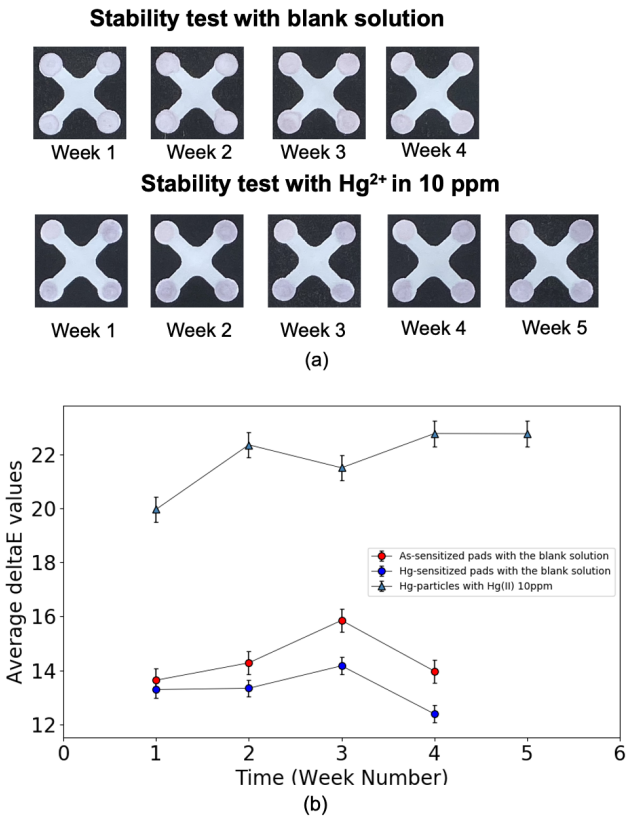

Figure 11. *The stability test results: (a) Test Images for the samples with blank solution and Hg^{2+} at 10 ppm (3 replicates per each test: upper right, lower left, and lower right), respectively, (b) Analytical results (No data was acquired with the blank solution at the end of Week 5.)*

Author Biography

Min Zhao *is a Ph.D. candidate in Electrical and Computer Engineering at Purdue University working under the supervision of Professor Jan P. Allebach. She received her B.S. degree in Mechanical Engineering from Qingdao Technology University, Shandong, China. Now, her current research interests include bio-printing and image analysis.*

Susana Diaz-Amaya*, Ph.D.(c) in materials engineering at Purdue University with a bachelor's degree in microbiology from the Pontifical Javeriana University, Colombia. Susana joined the University of Tolima as an assistant professor in 2011, and started her industrial career, serving as leader of R&D for the agroindustry and as an independent consul-*

tant for 5 years. Her current research interest is focused on the design and fabrication of low-cost, novel nanomaterials for high-throughput manufacturing of biosensing platforms.

***Amanda Deering** is a clinical assistant professor of Food Science at Purdue University. Her research focuses on examining the internalization of human pathogenic bacteria in plants, and routes of contamination that can contribute to plants harboring pathogenic bacteria. Amanda also works closely with industry to develop and test novel sanitization treatments that can be used for fresh produce, and works directly with Indiana fruit and vegetable growers to address food safety issues on the farm.*

***Lia Stanciu** is a professor of Materials Engineering at Purdue University. She earned her Ph.D. in Materials Science from U.C. Davis in 2003. In 2005, she joined Purdue's School of Materials Engineering as a faculty member. Her main research areas include advanced biomaterials for implantation, materials for biosensing devices and nanotechnology.*

***George T. Chiu** is a professor of Mechanical Engineering with courtesy appointments in Electrical and Computer Engineering and Psychological Sciences at Purdue University. He received the B.S. degree from National Taiwan University and the M.S. and Ph.D. degrees from University of California at Berkeley. His research interests are mechatronics and control with applications to digital printing and imaging systems, digital fabrications and functional printing. He is a Fellow of ASME and IS&T.*

***Jan P. Allebach** is Hewlett-Packard Distinguished Professor of Electrical and Computer Engineering at Purdue University. Allebach was named Electronic Imaging Scientist of the Year by IS&T and SPIE, and was named Honorary Member of IS&T, the highest award that IS&T bestows. He has received the IEEE Daniel E. Noble Award, the IS&T/OSA Edwin Land Medal, is a Fellow of the National Academy of Inventors, and is a member of the National Academy of Engineering.*

JOIN US AT THE NEXT EI!

IS&T International Symposium on

Electronic Imaging

SCIENCE AND TECHNOLOGY

Imaging across applications . . . Where industry and academia meet!

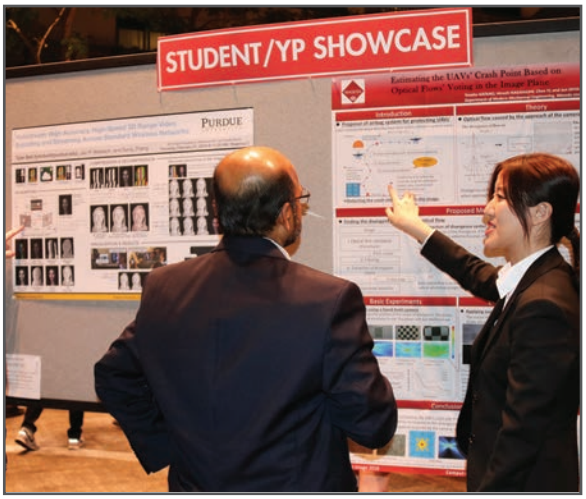

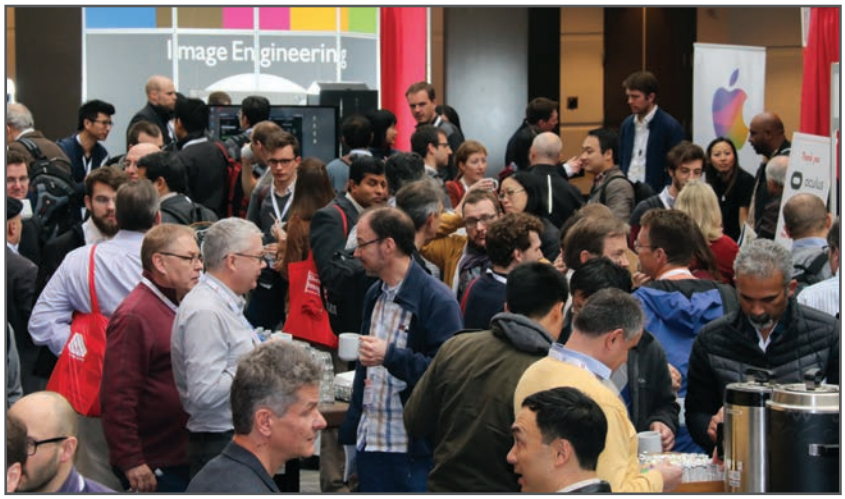

• SHORT COURSES • EXHIBITS • DEMONSTRATION SESSION • PLENARY TALKS •
• INTERACTIVE PAPER SESSION • SPECIAL EVENTS • TECHNICAL SESSIONS •

www.electronicimaging.org

IS&T
imaging.org